08

Synthesis of arrays nanostructured porous silicon wires in electron conductivity type silicon with crystallographic orientation (111)

© A.Yu. Gagarina,[1] L.S. Bogoslovskaya,[1] Yu.M. Spivak,[1] K.N. Novikova,[2] A. Kuznetsov,[1] V.A. Moshnikov[1]

[1] St. Petersburg State Electrotechnical University „LETI"
197376 St. Petersburg, Russia
[2] St. Petersburg National Research Academic University named after Zh.I. Alferov RAS,
194021 St. Petersburg, Russia
e-mail: gagarina.au@gmail.com

The method of modified metal-assisted electrochemical etching was proposed and arrays of nanostructured porous silicon wires on n-type monocrystalline silicon substrate with crystallographic orientation (111) were obtained. The influence of the electrolyte composition at the second stage of obtaining on the morphology of silicon wires by scanning electron microscopy methods was revealed. The phase composition of porous silicon wires was controlled by Raman spectroscopy.

Keywords: Porous silicon, porous Silicon nanowires, MACE, Nanomaterials, Raman spectroscopy.

Introduction

Nanostructured porous silicon wires (NPSW) are a promising material for modern science and technology, as they demonstrate great potential for application in such areas of micro- and nanoelectronics as biosensorics [1–4], gas sensorics [5–8], solar energy [9–11] and systems for targeted delivery of drug substances [12–14]. NPSW arrays are promising as antireflection coatings for solar cells. It was experimentally established that in the region of short wavelengths (less than 500 nm) the reflection coefficient is about 5%. As the range increases to 800 nm, the reflectance decreases down to 1% [15–17]. Nanostructured porous silicon nanowires are also of great interest for microfluidics, where the possibility of providing superhydrophobic or hydrophilic properties to material [18,19] comes to the first plan. The superhydrophobic surface allows liquid droplets to be moved by means of small forces due to the small contact of the droplet with the surface and, consequently, the low resistance to its movement. This property is also used to create self-cleaning or antibacterial surfaces. The surface provision with hydrophilic properties, together with the biocompatibility and biodegradability of this texture, makes it an excellent material for targeted drug delivery, implants and dressings [20–23]. One of the possible applications of nanostructures based on porous silicon (PS) are cathodes with low threshold emission [24].

Sensorics is one of the most relevant areas of NPSW application. Modern gas sensors based on metal oxides demonstrate a fast and reproducible response to changes in the concentration of detected gases, however, the operating temperatures of such sensors vary in the range of $200-600°C$ [25,26]. The advantages of NPSW-based sensors are due to the fact that they are compatible with large-scale integration processes, have excellent dynamic response and recovery characteristics, high selectivity and low operating temperatures, and varying their physicochemical properties is possible by changing the technological conditions of synthesis and does not require additional financial costs. [27–29]. One of the effective ways to increase the sensitivity and reduce the response/recovery time of such nanostructures is the functionalization of metals and metal oxides with nanoparticles. Thus, the functionalization of NPSW with catalytically active nanoparticles Au [30,31], Ag [32,33], Pd [34–37], and Pt [38,39] makes it possible to detect gaseous hydrogen in the range from 15 to 1 ppm [37,38]. Some papers [32,33] demonstrated the possibility of using composites based on silicon nanowires and Ag nanoparticles to detect NO_2 (at 0.3 ppm level) and NH_3 (at level 10 ppm) at room temperature in air. In this case, the response increasing by three times was observed compared to non-functionalized nanostructured silicon wires (NSWs) and its recovery for $2-9$ s at NH_3 concentrations from 0.33 to 10 ppm [33]. Also, composites based on silicon nanowires and metal oxide semiconductors, for example, ZnO, SnO_2, TiO_2, WO_3, are actively studied to determine in atmosphere of such gases as CH_4 [40] and NO_2 [41]. It was determined that the shape, size, and structure of the „guest" in the porous silicon matrix affect the sensitivity and selectivity with respect to certain gases. For example, in the paper [41] the possibility of implementing a sensor based on NSW and ZnO nanowires, which has a high sensitivity to NO_2, was demonstrated. In this case, the response values of the sensor turned out to be relatively low at concentrations of $5-50$ ppm of the detected gas. However, the ZnO deposition on the NSW in the form

of a nanograined film [42] made it possible to obtain a high and fast response to NO up to 2 ppm. This indicates the possibility of the parameters control depending on the way the porous matrix is functionalized.

Nevertheless, commercialization and introduction of NPSW into production are currently difficult due to the insufficiently developed technology for the NPSW synthesis for mass production. Most of the existing technologies require expensive equipment, are characterized by laboriousness of the technological process and low purity of the synthesized material. One of the most common (due to low cost and high manufacturability) methods for the NPSW synthesis is metal-assisted chemical etching (MACE). However, this method is severely limited in the choice of the resistivity of the initial plate, since the porous structure of the wires can be realized only at high doping levels p-Si with (100) crystal-lattice orientation. Hence, special interest arises in the possibility of synthesizing the structure on substrates with a wider range of resistivity and other crystal-lattice orientations, in particular (111). The latter is especially actual, since the (111) plate anodizing allows one to obtain a highly porous „fir-tree" structure with a system of pores well-branched and predominantly oriented along $\langle 100 \rangle$ [43,44]. At the same time, the NPSW synthesis on silicon substrates with (111) orientation is complicated by the specifics of anisotropic etching of single-crystal silicon. The crystallographic direction in silicon with the highest etching rate is $\langle 100 \rangle$, therefore, regardless of the chosen substrate orientation, under the chosen modes, the silicon etching in this direction will always proceed more intensively. Therefore, there is a need to stimulate the etching process.

The aim of this paper is to develop method for the porous nanorods formation on n-Si (111) using modified metal-stimulated electrochemical etching of single-crystal silicon.

1. Method of NPSW production

It was proposed to carry out the synthesis of single-crystal silicon grade KEF-4.5(111) with a thickness of $460 \mu m$ by a two-stage modified method of metal-activated electrochemical etching (MAECE). The synthesis scheme is shown in Fig. 1.

At the first stage the intermediate nanocomposite based on porous silicon and Ag is obtained. In one technological step a layer of porous silicon is formed, and silver nanoparticles are deposited on its surface from aqueous-alcoholic solution of a silver-containing salt. With given technological parameters (Table 1) the layer of porous silicon is characterized by a depth of $15-20 \mu m$ and a predominant growth of pores in the $\langle 100 \rangle$ direction. Previously, it was experimentally identified that Ag nanoparticles are deposited on the surface of porous silicon only and do not go into pores [45].

At the second stage, the porous silicon/Ag composite is electrochemically etched in the aqueous-alcoholic solution
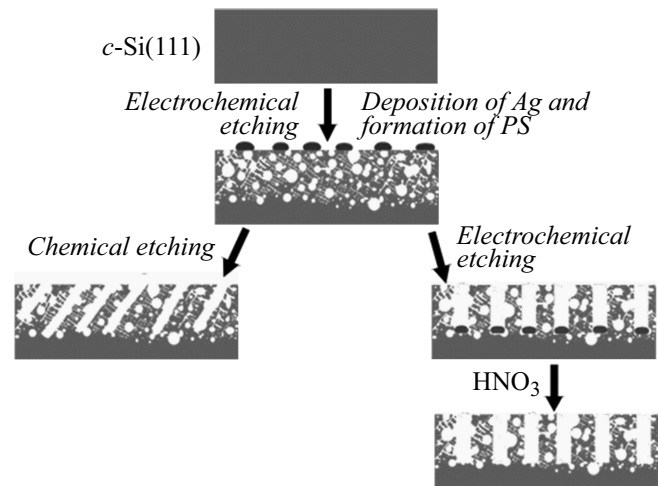

Figure 1. Scheme for NPSW synthesis on silicon with crystal-lattice orientation (111): on the left — classical MACE method; on the right — MAECE method.

of hydrofluoric acid. Ag nanoparticles act as a catalyst, due to which Si regions, that are in contact with Ag, are oxidized to SiO_2 and are more intensely etched by fluorine ions. The variable parameters were the electrolyte composition and the anodizing time.

2. Physical methods of samples study

The morphology of the obtained samples was studied by scanning electron microscopy (SEM) using device FEI Quanta with a typical magnification of $3.000^{\times} - 8.000^{\times}$ and accelerating voltage values in the range of $20.000 - 25.000$ kV. The elements distribution over selected areas of the surface was analyzed from the values of the intensities of the characteristic X-ray radiation using the method of energy-dispersive X-ray spectroscopy.

Data on the structure and phase composition of the samples were obtained by Raman microscopy. Raman spectra were recorded in backscattering geometry at room temperature using a Horiba LabRAM HR 800 Raman spectrometer equipped with a confocal microscope. The wavelength of the exciting radiation was 532 nm. All measurements were performed at room temperature.

3. Results and discussion

3.1. Samples examination by scanning electron microscopy

3.1.1. Study of sample morphology at the first technological stage

At the first technological stage a layer of porous silicon is formed, and silver nanoparticles (PS/Ag) are simultaneously deposited on the porous silicon surface. By varying the

Table 1. Technological parameters of NPSW synthesis

№	First stage			Second stage		
	j, mA/cm^2	t, min	Electrolyte	j, mA/cm^2	t, min	Electrolyte
1					20	$C_3H_8O:HF:H_2O$ (2:1:1)
2					40	$C_3H_8O:HF:H_2O$ (2:1:1)
3	15	4.5	$C_3H_8O:HF:H_2O:AgNO_3$	180		$C_3H_8O:HF:H_2O^*$ (2:1:1)
4					20	$C_3H_8O:HF:H_2O:H_2O_2$ (2:1:1:0.001)
5						$HF:H_2O:C_3H_8O:HNO_3$ (2:1:1:0.03)
6						$HF:H_2O_2$ (1:1)

Note. * After the second stage, additional chemical etching was carried out.
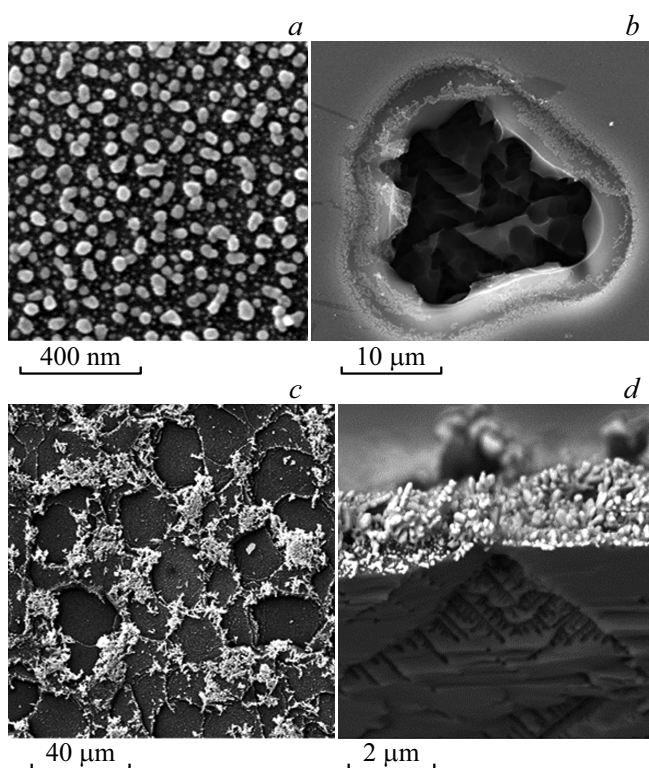
Figure 2 images (a, b, c, d)

Figure 2. SEM images of PS/Ag composites at various concentrations of $AgNO_3$ in the electrolyte: a, b — at 0.02 M; c, d — at 0.5 M; a, c — image of the PC/Ag composite surface, b — image of single pore, top view, d — transverse chip of PC/Ag composite at $AgNO_3$ concentration 0.5 M.

$AgNO_3$ concentration in the electrolyte and the anodization time, both island deposition of nanoparticles and the formation of dendrites are possible (Fig. 2). The morphology of the formed layer of porous silicon in this case is determined by two factors: the crystal-lattice orientation of the plate and the anodizing current density.

The results of electron microprobe analysis (EMPA) (Fig. 3) confirm the silver absence in the pores of the silicon matrix after the first technological stage.

3.2. Study of sample morphology at the second technological stage

3.2.1. Investigation of anodizing time effect on samples morphology

Fig. 4, a, b shows the SEM images of NPSW samples obtained with the same electrolyte compositions but different anodization times, 20 and 40 min, respectively.

With anodizing time of 20 min the average height of the NPSW was 30 μm; if the anodizing time increases to 40 min, the average height of the wires increases to 40 μm. The dependence of the height of nanostructured wires on the anodizing time is non-linear, which is associated with the decreasing of the pore surface wettability with buffer solution as the structure deepens, and etching of the side channels of the pores. Another factor that slows down the growth of NPSW is the difference in the rates of growth and etching of SiO_2 in HF. The oxide growth rate in the $\langle 111 \rangle$ direction is higher than its etching rate.

The wires along the entire height have a well-developed porous structure with pores predominant formation in the $\langle 100 \rangle$ direction. Despite the absence of post-processing operations, silver nanoparticles were not detected between the wires.

3.2.2. Investigation of post-processing effect on samples morphology

At the end of the second stage of MAECE, sample 3 was additionally subjected to chemical etching in aqueous' alcohol solution of HF for 48 h. SEM images confirm the absence of wire structure (Fig. 4, c, d). This is presumably due to the fact that as a result of the anisotropic nature of chemical etching due to the pores predominant formation in $\langle 100 \rangle$ direction, the wire structure became mechanically unstable and subjected to significant deformations. The thickness of the porous layer was about 31 μm. Such porous silicon is a mechanically stressed structure and can be used to obtain nanosized porous silicon powders for theranostics and imaging systems.
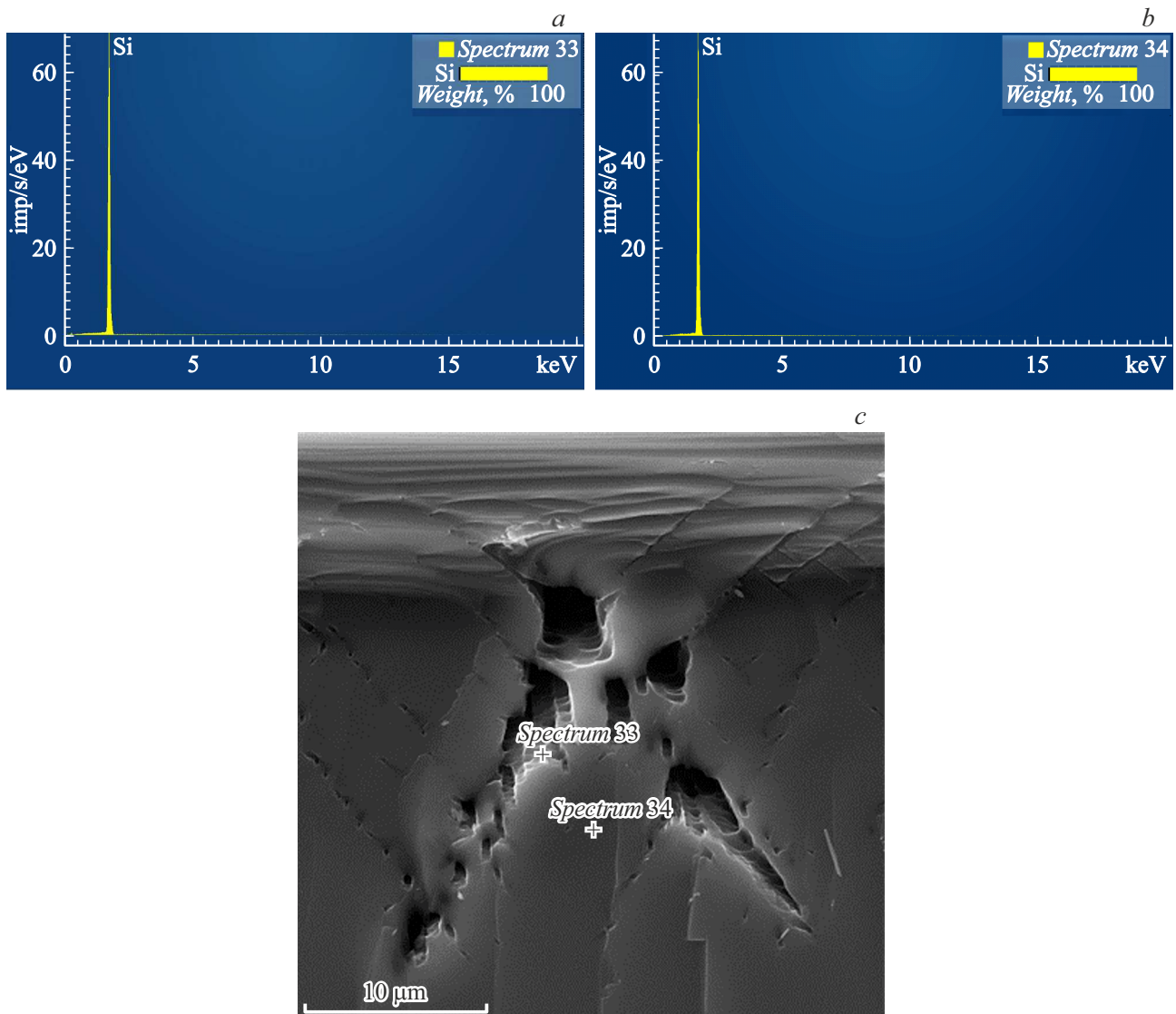
Figure 3. *a* — X-ray spectra of characteristic radiation for the PS/Ag composite, *b* — SEM image of chip of PS/Ag composite.

3.2.3. Investigation of electrolyte composition effect on samples morphology

In this part of this paper we studied the effect of the oxidizer type on the morphology of the synthesized nanostructure. H_2O, H_2O_2, and HNO_3 were considered as oxidizers. Aqueous alcohol solution of HF was used as the main electrolyte. $H2O_2$ and HNO_3 are more reactive compounds and strong oxidizers than H_2O, and it was assumed that the process of the nanostructured wires formation would proceed more intensively for all additives, which would help to reduce the anodization time to achieve a similar morphology.

However, if H_2O_2 is added to the initial electrolyte, the total oxidizer concentration increasing resulted in nonselective etching increasing and, as a consequence, to the formation of the „fir tree" type structure, characteristic for plates with crystal-lattice orientation (111), (Fig. 4, *e, f*), formed during anodic dissolution.

When using electrolyte with the addition of an aqueous solution of HNO_3, it was possible to synthesize a porous structure heterogeneous through height with clearly distinguishable vertical channels (Fig. 4, *g, h*). The height of the wire-like structure varied from 8 to $21\,\mu m$. HNO_3 partially reacts with silver to form a soluble $AgNO_3$ product, which leads to the decreasing of surface concentration of silver particles and of the points of catalytically enhanced local oxidation on the silicon plate. It is also possible to cycle the processes of oxidation and recovery of silver, which slows down the rate of NPSW formation.

Sample 6 was synthesized using the electrolyte based on H_2O_2 and aqueous solution of HF with higher content of the etching agent (HF). Fig. 4, *i, j* shows SEM images of sample chips obtained at different angles. In this case, the formation of a two-level structure is observed,
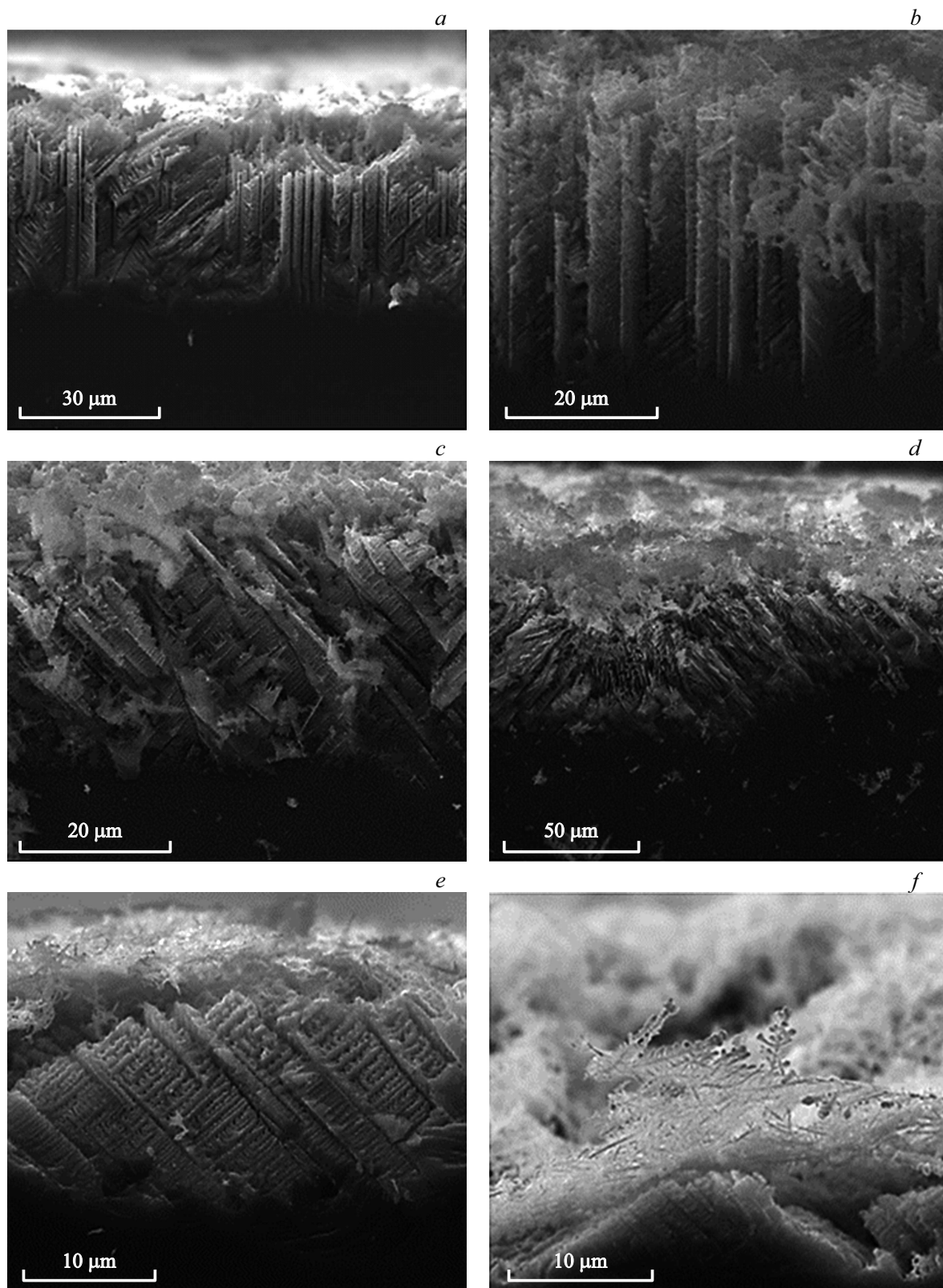
Figure 4. SEM images of cross sections: a — sample obtained with electrolyte composition $C_3H_8O:HF:H_2O$ ($t_a = 20$ min); b — sample obtained with electrolyte composition $C_3H_8O:HF:H_2O$ ($t_a = 20$ min); c, d — sample obtained with electrolyte composition $C_3H_8O:HF:H_2O$ with additional post-processing ; e, f — of the sample obtained with the electrolyte composition $C_3H_8O:HF:H_2O:H_2O_2$; g, h — sample obtained with electrolyte composition $HF:H_2O:C_3H_8O:HNO_3$; i, j — sample obtained with electrolyte composition $HF:H_2O_2$.
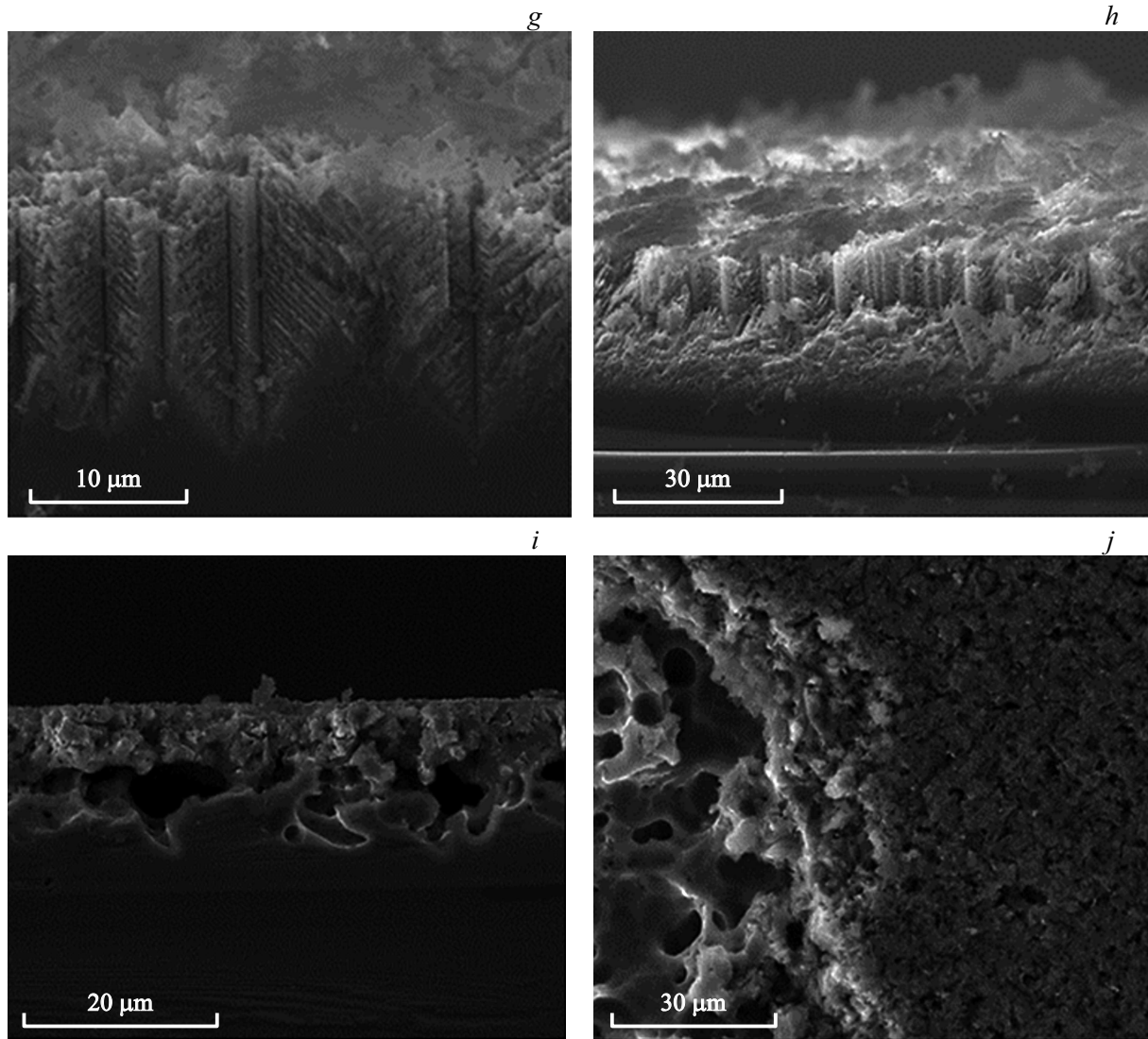
Fig. 4 (*continued.*)

presumably consisting of reaction products and disordered large channels-cavities in the layer of porous silicon. At the same time, no dendritic structure is observed on the surface of the sample, which was recorded for samples 1, 2 and 4.

It is known that varying of H_2O_2 concentration can change (increase) the rate of etching in depth and change the density of nanostructured wires [46,47]. In the present paper H_2O_2 concentration was less than 1%, which turned out to be insufficient for the formation of a vertical NPSW array. It is assumed that, at low concentrations of H_2O_2 etching to depth is limited by the formation of a thick layer of porous silicon both on the substrate surface and under particles of the catalytically active metal. The formation of the layer of porous silicon promotes the formation of areas strongly depleted of charge carriers, and therefore etching itself is possible only through the charge carriers transfer, which means the termination of oriented mass transfer induced by Ag nanoparticles. However, the nature of such a mechanism is still debatable.

Hence, we can conclude that the following statement is true for H_2O_2: the formation of the NPSW array is carried out at H_2O_2 concentrations above the threshold value ($\sim 5\%$).

3.3. Examination of samples by Raman spectroscopy

Fig. 5 shows the Raman spectrum for NPSW at different laser radiation powers in the range of $460-560\,cm^{-1}$. In this case, for the optical phonon mode of the first order, a strong shift to the low-frequency region is observed with laser radiation power increasing.

Table 2 lists the values of the Raman shift for the TO-mode. It is known that high laser power can promote a local temperature increasing in a nanostructured silicon matrix and affect the shift of the entire Raman spectrum [48]. For bulk single-crystal silicon, this effect is insignificant. This feature can be related to the lower thermal conductivity
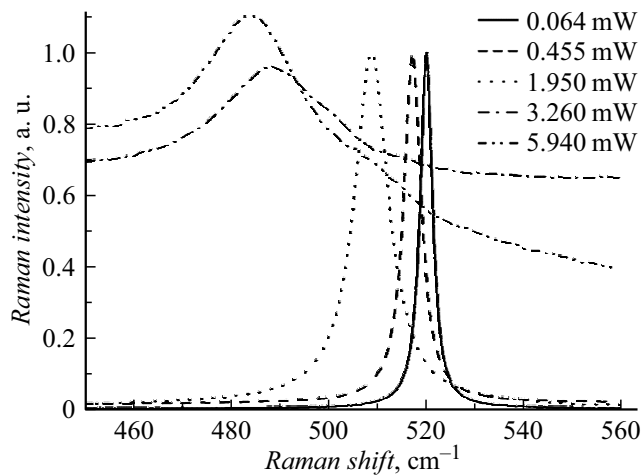
Figure 5. Raman spectra for NPSW in the region $520 \, cm^{-1}$ for different powers of laser irradiation of the sample. The accumulation time was 15 s.

Table 2. TO-mode position vs. the laser radiation power

Power, mW	0.064	0.4555	1.95	3.26	5.94
Raman shift, cm^{-1}	520.08	517.17	508.93	488.53	483.24

Table 3. Change in position of optical phonon mode of the first order after irradiation with laser of various powers

Power, mW	0.064	0.4555	3.26	5.94
Raman shift, cm^{-1}	520.08	520.1	519.11	519.59

of wire silicon nanostructures [49] as compared to single-crystal Si due to the complex phase composition and porous structure.

It is assumed that the strong dependence of the Raman shift on the laser radiation power is associated with local heating of the nanostructure and the subsequent appearance of mechanical stresses at the hot point, as it is evidenced by strong shifts to lower energies area.

In order to determine whether recrystallization processes are observed for such a structure, it was proposed to measure the spectrum of the nanostructure at the same point after measurement at increased power values, but at a power of 0.064 mW (Fig. 6). In this case, for all points an insignificant (Table 3) shift of the main silicon peak was observed, which can be associated either with the appearance of mechanical stresses characteristic for the porous silicon structure, or with extremely insignificant recrystallization processes occurring in the near-surface layers of the nanostructure.

The first assumption is supported by the fact that at low pumping power, no change in the shape and half-width of the peaks was observed, for example, the appearance of a wide shoulder at $480 \, cm^{-1}$ or an asymmetric band

near $400 \, cm^{-1}$, which usually indicate the formation of an amorphous phase [50] and Si−O−Si bonds [51,52], respectively.

However, the analysis at power of 0.064 mW cannot be considered absolutely reliable, because due to the low power density the received signal from other phonon modes turned out to be slightly distinguishable against the background of the fundamental silicon mode at $520 \, cm^{-1}$. Besides, as it is known from previous studies [53], the porous silicon obtained by the method described in this paper has a complex phase composition and contains amorphous, oxide, and nanocrystalline phases formed as a result of the disproportionation reaction near pores. Therefore, for further analysis of the synthesized nanostructures, 0.455 mW was chosen as the optimal power value, for which the minimum shifts of the fundamental TO-mode relative to single-crystal silicon were observed.

It can be seen from Fig. 7 that the entire NPSW spectrum is characterized by a shift to the low-wavelength region.
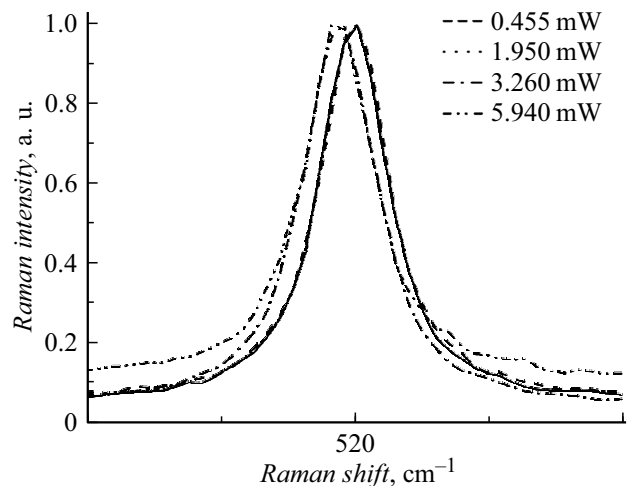

Figure 6. Raman spectra for NPSW in the region $520 \, cm^{-1}$ after sample irradiation by laser with various power. Radiation power is 0.064 mW, accumulation time is 15 s.
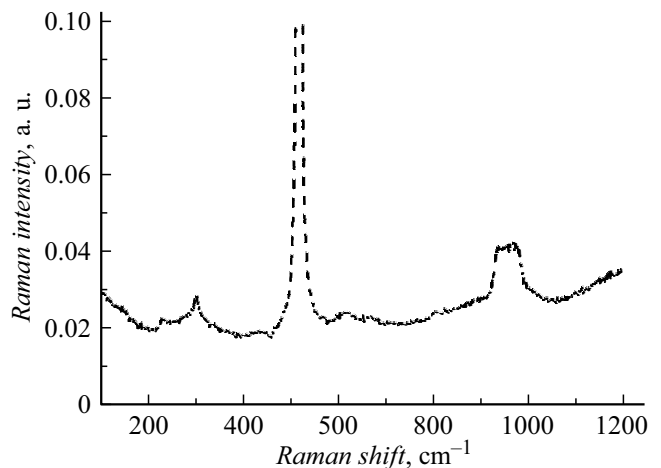

Figure 7. Raman spectra for NPSW at laser power 0.455 mW.

According to [55], the magnitude of mechanical stress can be estimated by the formula

$$\sigma = -52.71\Delta\omega,$$

where $\Delta\omega$ is the difference between the positions of the maximum of the first-order spectral line for silicon in the absence of mechanical stresses and the position of the corresponding maximum for the nanostructure. Hence, for shift of $520.1\,\mathrm{cm}^{-1}$, the mechanical stress will be $47.4\,\mathrm{MPa}$.

One can also note the amorphous phase presence at $610\,\mathrm{cm}^{-1}$ [55,56], and an oxide phase presence, as it is evidenced by the appearance of band at $432\,\mathrm{cm}^{-1}$ associated with vibrations of the $Si-O-Si$ intertetrahedral bond [52,55,56]. The broadening of the spectral line in the region of $520\,\mathrm{cm}^{-1}$ for NPSW is explained by the effect of spatial limitation of phonons, which occurs as a result of the disproportionation reaction and precipitation of silicon in the form of nanosized crystallites [52,57–60].

The results of Raman spectroscopy indicate that NPSW contains crystalline, nanocrystalline and amorphous phases, which is in good agreement with the general ideas about NPSW: a crystalline core, in the pores of which silicon nanocrystals (including quantum dots) are present, on the surface of the structure — layers of amorphous silicon and silicon oxide.

Conclusion

A new technique for the NPSW array formation in *n*-Si with (111) crystal-lattice orientation, which includes two stages was proposed and tested. At the first stage, by electrochemical anodizing of single-crystal silicon in an aqueous-alcoholic solution of hydrogen fluoride containing $AgNO_3$ a preliminary structure is simultaneously formed, which is a layer of porous silicon with dendrites or island structures of Ag on the surface. At the second stage the preliminary structure is subjected to electrochemical anodic dissolution with the NPSW formation with a controlled arrangement of pores.

The study of the morphology and composition of the preliminary PS/Ag structures by SEM and EPMA showed that during the structure formation the silver particles are deposited only on the surface of the porous silicon layer and do not penetrate deep into the pores. Depending on the time of anodization and the concentration of the silver-containing salt, the formation of both silver islands and dendrites is possible.

A study of the NPSW synthesis conditions at the second stage showed that the most optimal conditions are the formation of a system of porous nanowires with a standard electrolyte composition $(C_3H_8O\colon HF\colon H_2O)$, current density value equal to $180\,\mathrm{mA/cm}^2$, and anodizing time from $20\,\mathrm{min}$. When an additional oxidizer is added, it is possible to form both „fir tree" structure and a wire-like structure.

Using Raman spectroscopy methods, it was shown that NPSW formed using modified metal-activated electrochemical etching represent an array of wires with a crystalline core, which is covered with layers of amorphous and oxidized silicon; as a result of the disproportionation reaction silicon nanocrystals are formed near the pores.

Conflict of interest

The authors declare that they have no conflict of interest.

References

[1] S. Chen, Y. Tang, K. Zhan, D. Sun, X. Hou. Nano Today, **20**, 84−100 (2018). DOI: 10.1016/j.nantod.2018.04.006

[2] O. Žukovskaja, S. Agafilushkina, V. Sivakov, K. Weber, D. Cialla-May, L. Osminkina, J. Popp. J. Talanta, **202**, 171−177 (2019). DOI: 10.1016/j.talanta.2019.04.047

[3] M.B. Gongalsky, U.A. Tsurikova, J.V. Samsonova, G.Z. Gvindzhiliiia, K.A. Gonchar, N.Y. Saushkin, A.A. Kudryavtsev, E.A. Kropotkina, A.S. Gambaryan, L.A. Osminkina. Res. Mater., 6, 100084 (2020).
DOI: 10.1016/j.rinma.2020.100084

[4] A.D. Kartashova, K.A. Gonchar, D.A. Chermoshentsev, E.A. Alekseeva, M.B. Gongalsky, I.V. Bozhev, A.A. Eliseev, S.A. Dyakov, J.V. Samsonova, L.A. Osminkina. ACS Biomater. Sci. Eng., **8** (10), 4175−4184 (2022).
DOI: 10.1021/acsbiomaterials.1c00728

[5] Y. Qin, Y. Wang, Y. Liu, Y.J. Mater. Sci. Mater. Electron., **27** (11), 11319−11324 (2016).
DOI: 10.1007/s10854-016-5255-1

[6] Y. Wang, M. Hu, Z. Wang, X. Liu, L. Yuan. Mater. Sci. Semicond. Process., **56**, 307−312 (2016).
DOI: 10.1016/j.mssp.2016.09.002

[7] L. Pichon, A.C. Salaün, G. Wenga, R. Rogel, E. Jacques. Procedia Eng., **87**, 1003−1006 (2014).
DOI: 10.1016/j.proeng.2014.11.329

[8] L. Pichon, R. Rogel, E. Jacques, A.C. Salaun. Phys. Status Solidi, **11**, 344−348 (2014). DOI: 10.1002/pssc.201300206

[9] G. Otnes, M.T. Borgström. Nano Today, **12**, 31−45 (2017). DOI: 10.1016/j.nantod.2016.10.007

[10] G.Y. Abdel-Latif, M.F.O. Hameed, M. Hussein, M.A. Razzak, S.S.A. Obayya. J. Photon. Energy, **7** (4), 047501 (2017). DOI: 10.1117/1.JPE.7.047501

[11] F.M. Korany, M.F.O. Hameed, M. Hussein, R. Mubarak, M.I. Eladawy, S.S.A. Obayya, J. Nanophoton., **12** (1), 016019 (2018). DOI: 10.1117/1.JNP.12.016019

[12] D. Korolev, V. Postnov, I. Aleksandrov, I. Murin. Biomolecules, **11** (10), 1544 (2021).
DOI: 10.3390/biom11101544

[13] Yu.M. Spivak, A.O. Belorus, A.A. Panevin, S.G. Zhuravsky, V.A. Moshnikov, K. Bespalova, P.A. Somov, Yu.M. Zhukov, A.S. Komolov, L.V. Chistyakova, N.Yu. Grigorieva. ZhTF **88**, 9 (1394) (1403) (in Russian).
DOI: 10.21883/JTF.2018.09.46427.57-18

[14] M. Lv, S. Su, Y. He, Q. Huang, W. Hu, D. Li, C. Fan, S.T. Lee. Adv. Mater., **22** (48), 5463−5467 (2010).
DOI: 10.1002/adma.201001934

[15] M.B. Rabha, L. Khezami, A.B. Jemai, R. Alhathlool, A. Ajbar. J. Cryst. Growth, **462**, 35−40 (2017).
DOI: 10.1016/j.jcrysgro.2017.01.021

[16] S. Li, W. Ma, X. Chen, K. Xie, Y. Li, X. He, X. Yang, Y. Lei. Appl. Surf. Sci., **369**, 232−240 (2016). DOI: 10.1016/j.apsusc.2016.02.028

[17] M. Jeon, K. Kamisako. Mater. Lett., **63** (9−10), 777−779 (2009). DOI: 10.1016/j.matlet.2009.01.001

[18] Y. Chen, Z. Guo, J. Xu, L. Shi, J. Li, Y. Zhang. Mater. Res. Bull., **47** (7), 1687−1692 (2012). DOI: 10.1016/j.materresbull.2012.03.049

[19] R. Blossey. Nature Mater., **2** (5), 301−306 (2003). DOI: 10.1038/nmat856

[20] L. Canham. *Handbook of Porous Silicon* (Springer International Publishing, Berlin, 2014)

[21] Y.M. Spivak, A.O. Belorus, P.A. Somov, S.S. Tulenin, K.A. Bespalova, V.A. Moshnikov. J. Phys. Conf. Ser. **643**, 012022 (2015). DOI: 10.1088/1742-6596/643/1/012022

[22] Yu.M. Spivak, K.A. Bespalova, A.O. Belorus, A.A. Panevin, P.A. Somov, N.Yu. Grigorieva, L.V. Chistyakova, S.G. Zhuravsky, V.A. Moshnikov. Biotekhnosfera, **51**, 69 (75) (in Russian). DOI: 10.21883/JTF.2018.09.46427.57-18

[23] Y. Spivak. *Proc. of the 2018 IEEE International Conference on Electrical Engineering and Photonics* (St. Petersburg, Russia, 2018), p. 244−248. DOI: 10.1109/EExPolytech.2018.8564424

[24] R. Smerdov, A. Mustafaev, Y. Spivak, V. Moshnikov, I. Bizyaev, P. Somov, V. Gerasimov. Electronics, **10** (1), 1−13 (2021). DOI: 10.3390/electronics10010042

[25] A. Dey. Mat. Sci. Eng. B, **229**, 206−217 (2018). DOI: 10.1016/j.mseb.2017.12.036

[26] F. Hossein-Babaei, A. Amini. Sens. Actuat. B Chem., **194**, 156−163 (2014). DOI: 10.1016/j.snb.2013.12.061

[27] Y. Qin, Y. Liu, Y. Wang. ECS J. Solid State Sci. Technol., **5** (7), P380−P383 (2016). DOI: 10.1149/2.0051607

[28] A. Bobkov, V. Luchinin, V. Moshnikov, S. Nalimova, Y. Spivak. Sensors., **22** (4), 1530 (2022). DOI: 10.3390/s22041530

[29] V.A. Moshnikov, I. Gracheva, A.S. Lenshin, Y.M. Spivak, M.G. Anchkov, V.V. Kuznetsov, J.M. Olchowik. J. Non. Cryst. Solids, **358** (3), 590−595 (2012). DOI: 10.1016/j.jnoncrysol.2011.10

[30] L.B. Ahmed, S. Naama, A. Keffous, A. Hassein-Bey, T. Hadjersi. Prog. Nat. Sci., **25** (2), 101−110 (2015). DOI: 10.1016/j.pnsc.2015.03.003

[31] S. Naama, T. Hadjersi, A. Keffous, G. Nezzal. Mat. Sci. Semicond. Process., **38**, 367−372 (2015). DOI: 10.1016/j.mssp.2015.01.027

[32] Y. Qin, D. Liu, T. Zhang, Z. Cui. ACS Appl. Mater. Interfaces, **9** (34), 28766−28773 (2017). DOI: 10.1021/acsami.7b10584

[33] Y. Qin, D. Liu, Z. Wang, Y. Jiang. Sens. Actuat. B Chem., **258**, 730−738 (2018). DOI: 10.1016/j.snb.2017.11.177

[34] J. Baek, B. Jang, M.H. Kim, W. Kim, J. Kim, H.J. Rim, S. Shin, T. Lee, S. Cho, W. Lee. Sens. Actuat. B Chem., **256**, 465−471 (2018). DOI: 10.1016/j.snb.2017.10.109

[35] J.H. Ahn, J. Yun, D.I. Moon, Y.K. Choi, I. Park. Nanotechnology, **26** (9), 095501 (2015). DOI: 10.1088/0957-4484/26/9/095501

[36] J. Yun, J.H. Ahn, D.I. Moon, Y.K. Choi, I. Park. ACS Appl. Mater. Interfaces, **11** (45), 42349−42357 (2019). DOI: 10.1021/acsami.9b15111

[37] L.S. Zhu, J. Zhang, X.W. Xu, Y.Z. Yu, X. Wu, T. Yang, X.H. Wang. Sens. Actuat. B Chem., **227**, 515−523 (2016). DOI: 10.1016/j.snb.2015.12.080

[38] L.B. Ahmed, S. Naama, A. Keffous, A. Hassein-Bey, T. Hadjersi. Prog. Nat. Sci., **25** (2), 101−110 (2015). DOI: 10.1016/j.pnsc.2015.03.003

[39] S. Naama, T. Hadjersi, A. Keffous, G. Nezzal. Mater. Sci. Semicond. Process., **38**, 367−372 (2015). DOI: 10.1016/j.mssp.2015.01.027

[40] D. Liu, L. Lin, Q. Chen, H. Zhou, J. Wu. ACS Sens., **2**, 1491−1497 (2017). DOI: 10.1021/acssensors.7b00459

[41] J. Liao, Z. Li, G. Wang, C. Chen, S. Lv, M. Li. Phys. Chem. Chem. Phys, **18** (6), 4835−4841 (2016). DOI: 10.1039/C5CP07036H

[42] C. Samanta, A. Ghatak, A.K. Raychaudhuri, B. Ghosh. Nanotechnology, **30**, 305501 (2019). DOI: 10.1088/1361-6528/ab10f8

[43] V.A. Moshnikov, A.S. Lenshin, Yu.M. Spivak. *Issledovanie, tekhnologiya i ispol'zovanie nanoporistykh nositelej lekarstv v meditsine* (Khimizdat, SPb, 2015), s. 70−116. (in Russian)

[44] P.G. Travkin, N.V. Vorontsova, S.A. Vysotsky, A.S. Lenshin, Yu.M. Spivak, V.A. Moshnikov. Izv. (SPbGETU „LETI,"**4**, 3−9 (2011). (in Russian).

[45] Y.M. Spivak, A.Y. Gagarina, M.O. Portnova, A.V. Zaikina, V.A. Moshnikov. J. Phys. Conf. Ser., **1697**, 012126 (2020). DOI: 10.1088/1742-6596/1697/1/012126

[46] B. Moumni, A.B. Jaballah. Appl. Surf. Sci., **425**, 1−7 (2017).

[47] K.A. Gonchar, D.V. Moiseev, I.V. Bozhev, L.A. Osminkina. Mater. Sci. Semicond. Process., **125**, 105644 (2021).

[48] Y. Chen, B. Peng, B. Wang. J. Phys. Chem. C, **111** (16), 5855−5858 (2007). DOI: 10.1021/jp0685028

[49] S. Piscanec, M. Cantoro, A.C. Ferrari, J.A. Zapien, Y. Lifshitz, S.T. Lee, S. Hofmann, J. Robertson. Phys. Rev. B, **68** (24), 241312 (2003). DOI: 10.1103/physrevb.68.241312

[50] R. Tsu, H. Shen, M. Dutta. Appl. Phys. Lett., **60** (1), 112−114 (1992). DOI: 10.1063/1.107364

[51] R.K. Biswas, P. Khan, S. Mukherjee, A.K. Mukhopadhyay, J. Ghosh, K. Muraleedharan. J. Non. Cryst. Solids, **488**, 1−9 (2018). DOI: 10.1016/j.jnoncrysol.2018.02.037

[52] P. McMillan. Am. Mineral., **69** (7−8), 622−644 (1984).

[53] A.S. Len'shin, V.M. Kashkarov, Y.M. Spivak, V.A. Moshnikov. Glass Phys. Chem., **38** (3), 315−321 (2012). DOI: 10.1134/s1087659612030091

[54] Q. Li, W. Qiu, H. Tan, J. Guo, Y. Kang. Opt. Lasers Eng., **48** (11), 1119−1125 (2010). DOI: 10.1016/j.optlaseng.2009.12.020

[55] R.K. Biswas, P. Khan, S. Mukherjee, A.K. Mukhopadhyay, J. Ghosh, K. Muraleedharan. J. Non. Cryst. Solids, **488**, 1−9 (2018). DOI: 10.1016/j.jnoncrysol.2018.02.037

[56] A.V. Kononina, Yu.V. Balakshin, K.A. Gonchar, I.V. Bozh'ev, A.A. Shemukhin, V.S. Chernysh. Pis'ma v ZHTF, **48** (2), 11 (in Russian). DOI: 10.21883/PJTF.2022.02.51912.18989

[57] I. Iatsunskyi, S. Jurga, V. Smyntyna, M. Pavlenko, V. Myndrul, A. Zaleska. Proc. SPIE, **9132**, 913217 (2014). DOI: 10.1117/12.2051489

[58] M. Ivanda. *Raman Spectroscopy of Porous Silicon. Handbook of Porous Silicon* (Springer, 2018), p. 611−620. DOI: 10.1007/978-3-319-71381-6_120

[59] T.A. Harriman, D.A. Lucca, J.K. Lee, M.J. Klopfstein, K. Herrmann, M. Nastasi. Nucl. Instrum. Meth. B, **267** (8−9), 1232−1234 (2009). DOI: 10.1016/j.nimb.2009.01.021

[60] A.S. Kachko, V.A. Volodin, V.R. Vakhovsky. Vestnik NGU, **5** (1), (2010). (in Russian)